Journal of Alloys and Compounds 508 (2010) 147–151

Contents lists available at ScienceDirect

Journal of Alloys and Compounds

journal homepage: www.elsevier.com/locate/jallcom

Synthesis and magnetic properties of iron nanoparticles confined in highly ordered mesoporous carbons

Tai-Ming Zhang, Dong-Lin Zhao*, Li Yin, Zeng-Min Shen

State Key Laboratory of Chemical Resource Engineering, Beijing University of Chemical Technology, Beijing 100029, China

ARTICLE INFO

Article history:
Received 20 June 2010
Received in revised form 5 August 2010
Accepted 6 August 2010
Available online 19 August 2010

Keywords:
Magnetically ordered materials
Chemical synthesis
Transmission electron microscopy
X-ray diffraction
Magnetic measurements

ABSTRACT

The iron nanoparticles confined in highly ordered mesoporous carbons (OMCs) have been directly synthesized through a simple soft templating method by using resorcinol–formaldehyde (RF) as a carbon precursor, triblock copolymer Pluronic F127 as a template agent and hydrated iron nitrite as an iron source. This synthesis was carried out by the carbonization of the F127/$[Fe(H_2O)_9](NO_3)_3$/RF composites self-assembled in an acidic medium, which was generated from the self-hydrolysis of precursory salt. The effects of iron loading contents on the morphology, pore feature and magnetic properties of the iron nanoparticles confined in OMCs were characterized by the X-ray diffraction, transmission electron microscopy, nitrogen sorption and vibrating-sample magnetometer measurement. It was found that Fe^{3+} was captured by the network of F127/RF and further reduced into metallic Fe nanoparticles during the carbonization. The results showed that the carbon material exhibited highly ordered mesoporous structure, and the iron nanoparticles were uniformly confined in the OMC walls when the Fe/R molar ratio was around 0.1. The saturation magnetization *Ms*, remanent magnetization *Mr*, and coercivity *Hc* of the Fe/OMC composites increased with the increasing of Fe/R molar ratio. The Fe/OMC composites exhibited the soft ferromagnetic behavior and the magnetization parameters could be adjusted by the content of iron.

1. Introduction

Ordered mesoporous carbons (OMCs) reported in 1991 [1] have attracted significant interest [2–11] due to their structural regularity, large specific surface area, thermal stability, chemical inertness, biocompatibility, and many potential applications in the fields of absorption [12], separation [13], hydrogen storage [14], catalyst supports [15,16], biomedical engineering [17] and energy storage [18–22]. For further applications of OMCs, metal nanoparticles were employed into the OMCs to modify their properties and broaden applications in the fields of adsorption, catalysis, lithium-ion batteries, electrochemical capacitors and magnetic separation, etc. [23,24]. There are three possible locations of guest particles in the OMCs. The guest particles may be located inside the mesochannels, within the walls or at the external surfaces of the OMCs. The metal nanoparticles confined inside the mesochannels and within the walls of OMCs are effectively protected by OMCs from oxidation and consequently showing long-term stability. When the metal nanoparticles stay inside the mesochannels, they will cause the reduction of surface area and pore volume. Incorporation of guest nanoparticles inside the walls of OMCs is an effective way to overcome this drawback. Moreover, in such structure, the guest nanoparticles are embedded in carbon walls, so they are accessible to gas and liquid molecules which enter the mesochannels from outside media [25].

So far, there are generally two routes to insert nanoparticles into the OMCs. One route is incorporating metal and compound nanoparticles (Pt [26,27], Ru [28], SnO_2 [29,30], MnO_2 [31,32]) into the pre-synthesized OMCs using impregnation, adsorption or ion exchange methods. Another route is infiltration of an appropriate carbon precursor and metal source into the mesopores of the silica template, followed by thermal polymerization, carbonization and subsequent removal of the silica framework with HF or NaOH solution [33–38]. Nevertheless, the above routes are fussy, time-consuming and high cost multi-step synthesis procedures, including repeated impregnation with carbon and metal precursors and the removal of hard templates [23]. Meanwhile, the mesoporous materials containing Fe, Co, Ni magnetic nanoparticles have fascinating magnetic properties, and many applications including magnetic storage media, ferrofluids, and as magnetic carriers for drug targeting [36,39–42]. Yao et al. synthesized the magnetically separable Ni/OMCs with a highly ordered cubic structure by the carbonization of the F127/$[Ni(H_2O)_6](NO_3)_2$/RF composites self-assembled in an alkaline medium [23]. Li et al. prepared the

* Corresponding author at: State Key Laboratory of Chemical Resource Engineering, Beijing University of Chemical Technology, No.15 Bei Sanhuan East Road, Beijing 100029, China. Tel.: +86 10 64434914; fax: +86 10 64454912.
E-mail address: dlzhao@mail.buct.edu.cn (D.-L. Zhao).

0925-8388/$ – see front matter © 2010 Elsevier B.V. All rights reserved.
doi:10.1016/j.jallcom.2010.08.030

highly ordered Fe/OMCs using a soft templating route [24]. Xing et al. synthesized α-Fe-incorporated nanoporous carbon through nanocasting strategy by using ordered mesoporous silica as a hard template and sugar as a carbon source [39].

Herein, we employed a simple soft templating method to synthesize magnetic Fe nanoparticles confined in OMCs (Fe/OMCs) under an acidic medium generated from the self-hydrolysis of precursory salt. The magnetic Fe/OMCs were fabricated through the self-assembly of F127, resorcinol–formaldehyde (RF) polymer and $[Fe(H_2O)_9](NO_3)_3$. Wherein, RF was used as a carbon precursor, triblock copolymer Pluronic F127 as a template agent and $[Fe(H_2O)_9](NO_3)_3$ as an iron source. The effects of Fe loading contents on the morphology, pore feature and magnetic properties of Fe/OMCs were investigated.

2. Experimental

2.1. Chemicals

Triblock poly(ethylene oxide)-*b*-poly(propylene oxide)-*b*-poly (ethylene oxide) copolymer Pluronic F127 (M_w = 12,600, $PEO_{106}PPO_{70}PEO_{106}$) was purchased from Aldrich Corp., and resorcinol, formaldehyde and hydrated iron nitrite ($[Fe(H_2O)_9](NO_3)_3$) were purchased from Beijing Chemical Corp. All chemicals were analytical pure grade and were used as received without any further purification.

2.2. Synthesis

The synthesis compositions were in the range of resorcinol/formaldehyde/F127/$[Fe(H_2O)_9](NO_3)_3$ (molar ratio) = 1:2:0.013:0.05–0.20. The resulting composite was designated as Fe/OMC–M, M denoted the molar ratio of $[Fe(H_2O)_9](NO_3)_3$ to resorcinol (Fe/R) at the beginning of polymerization. In a typical preparation, 2.45 g F127 and 1.65 g resorcinol were dissolved absolutely in 14 g of ethanol/water (1/1 vol%) solution under magnetic stirring at room temperature (signed A). An appropriate amount of hydrated iron nitrate corresponding to Fe/resorcinol molar ratio equal to 0.05, 0.10, 0.15, 0.20 was dissolved in 7 g of ethanol/water (1/1 vol%) solution (signed B). When solution B turned to be a light brown solution, it was dropped into solution A. After stirring for 2 h, 2.3 mL of formaldehyde (37%) was subsequently added dropwise to the above solution containing F127, resorcinol and $[Fe(H_2O)_9](NO_3)_3O$. Followed by an additional 2 h stirring, the mixture was kept standing until it turned cloudy and began to separate into two layers. This two phase mixture was further kept aging for two days. Subsequently, the upper light layer was discarded while the lower dark phase was stirred overnight until a sticky monolith was formed. Finally, the monolith was dried in an oven at 90 °C for 12 h and carbonized at 800 °C for 2 h, with a heating rate of 1 °C/min from 25 to 400 °C and 5 °C/min from 400 to 800 °C under a nitrogen atmosphere, to obtain the Fe/OMCs.

2.3. Characterization

Powder X-ray diffraction (XRD) patterns were recorded on a Rigaku D/max-2500B2+/PCX system operating with Cu Kα radiation (λ = 1.5406 Å). For small-angle XRD measurement with $2\theta \leq 5^\circ$, the step width and acquisition time were 0.002° and 0.24 s, respectively, and for wide-angle XRD measurement 0.02° and 0.15 s were employed.

The transmission electron microscope (TEM) images were obtained using a Hitachi H-800 transmission electron microscope operating at 200 kV. The high resolution TEM (HRTEM) images were recorded on a JEOL JEM-3010 microscope operating at 300 kV. Before TEM observations, the samples were prepared by dispersing the products in ethanol with an ultrasonic bath for 10 min and then one drop of the resulting suspension was placed on a copper grid.

Nitrogen adsorption–desorption isotherms were measured with an ASAP 2010 Micromeritics Instrument at 77 K. Before the measurement, the samples were degassed at 473 K for 12 h. The specific surface areas were calculated using the Brunauer–Emmett–Teller (BET) equation in a relative pressure range between P/P_0 = 0.05–0.3. The pore size distribution was estimated from the desorption branch of the isotherm using the Barrett–Joyner–Halenda (BJH) method.

The magnetic properties of Fe/OMCs were measured at room temperature with a vibration sample magnetometer (VSM, Lakeshore, Model 7307).

3. Results and discussion

The small-angle XRD patterns of Fe/OMC composites with different iron loadings are presented in Fig. 1. As shown in Fig. 1, the Fe/OMC-0.05, Fe/OMC-0.10 and Fe/OMC-0.15 samples exhibit intense diffraction peaks at 2θ range of 0.8–1°, which can be indexed to [1 0 0] reflection of hexagonal mesostructure [24]. A sharp and narrow diffraction peak at 2θ = 0.89° can be observed for Fe/OMC-0.10, which indicates that this sample possesses well-ordered mesostructure. However, no obvious diffraction peak was detected in the Fe/OMC-0.20 sample, implying that the optimal ordering of the hexagonal mesostructure can be obtained when Fe contents around Fe/R = 0.1 and the ordering decreased as the Fe content was either greater or smaller than this ratio. In the Fe/OMCs synthesis, when iron precursor $[Fe(H_2O)_9](NO_3)_3$ was added into the reaction mixture containing resorcinol–formaldehyde (RF) and F127, the acid was generated due to the hydrolysis of precursory salt. And it could be used as the catalyst for cross-linking between resorcinol and formaldehyde. The excess iron loading might disturb the self-assembly process and thus influence the final ordering of the mesostructure [24].

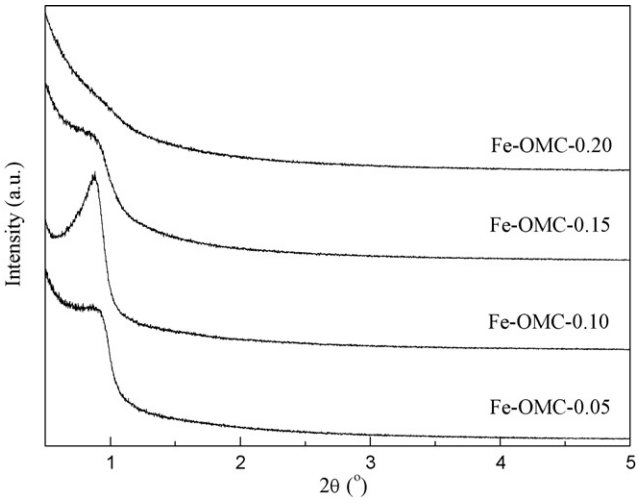

Fig. 1. Small-angle XRD patterns of Fe/OMC composites with different iron loadings.

Fig. 2 shows the wide-angle XRD patterns of Fe/OMC composites with different iron loadings. The wide-angle XRD patterns exhibit resolved diffraction peaks at 2θ = 44.7° for all samples, which are in accordance with the (1 1 0) diffraction of body-centered cubic (bcc) α-Fe (JCPDS card No. 06-0696). It indicates that Fe^{3+} was captured by the network of F127/RF and further reduced into metallic Fe nanoparticles during the carbonization. The weak diffraction peaks at 35.8° of Fe/OMC-0.05 and Fe/OMC-0.10 samples are in accordance with the (3 1 1) diffraction of γ-Fe_2O_3 (JCPDS card No.

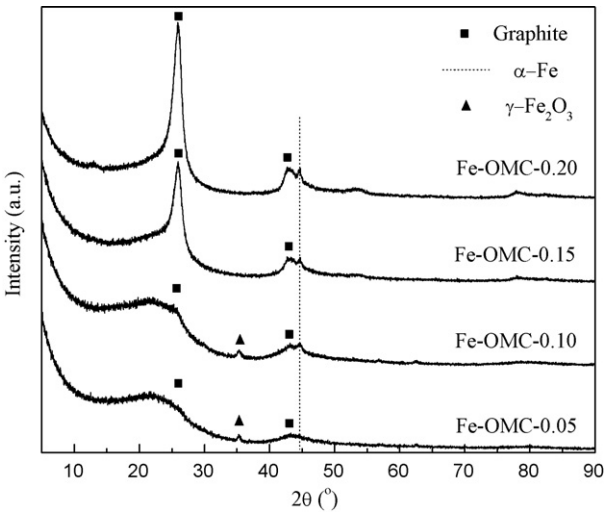

Fig. 2. Wide-angle XRD patterns of Fe/OMC composites with different iron loadings.

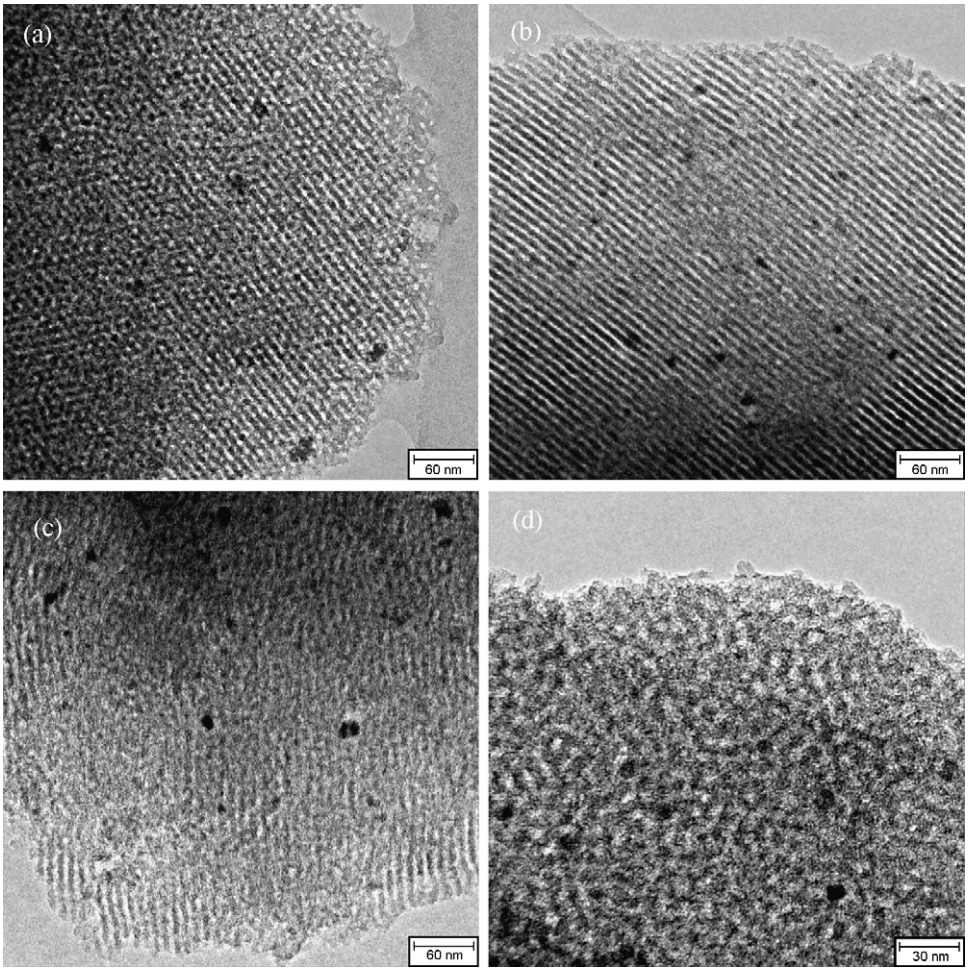

Fig. 3. TEM images of Fe/OMC composites with different iron loadings (a) Fe/OMC-0.05, (b) Fe/OMC-0.10, (c) Fe/OMC-0.15, and (d) Fe/OMC-0.20.

00-039-1346). The existence of γ-Fe_2O_3 may be due to the fact that metallic Fe possesses extremely high reactivity and thus some Fe nanoparticles exposed on the OMC surface can be easily oxidized to iron oxides when exposed in the air. In addition, when the Fe/R molar ratio were increased to above 0.1, an intensive diffraction peak at $2\theta = 26^\circ$, along with a resolved diffraction peak at $2\theta = 43^\circ$ can be seen in the resulting Fe/OMC composites, which can be indexed to the (0 0 2) and (1 0 1) diffraction peaks for typical graphite-like carbon. The interlayer spacing value (d spacing) of the (0 0 2) plane is 0.341 nm, a slightly bigger than the value (0.335 nm) of graphite [43], suggesting that the materials were well graphitized by the Fe nanoparticles during carbonization. It is well known that the nanosized transition metals such as Fe, Co, Ni can accelerate the development of graphitic structure (called catalytic graphitization) of carbon when they are heat-treated together with carbon materials in inert gas atmosphere [44–46].

TEM was used to directly observe the mesostructure of carbon and the distribution state of iron nanoparticles confined in the OMCs. Fig. 3 shows the typical TEM images of the Fe/OMC composites with different iron contents. As shown in Fig. 3, the parallel

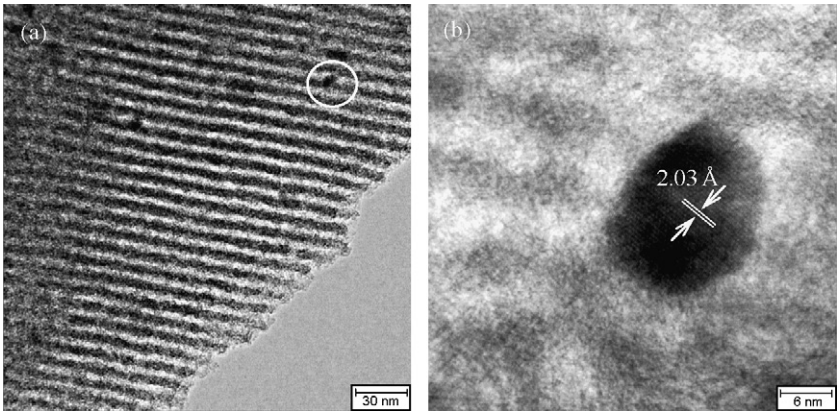

Fig. 4. Typical TEM image and corresponding HRTEM image of α-Fe particle confined in OMC (Fe/OMC-0.10).

Table 1
Textural properties of the Fe/OMC composites.

Sample name	Unit cell parameter[a] (nm)	BET surface area[b] ($m^2\ g^{-1}$)	Micropore surface area[c] ($m^2\ g^{-1}$)	Average size[d] (nm)	Pore Volume[e] ($cm^3\ g^{-1}$)	Pore wall thickness[f] (nm)
Fe/OMC-0.05	11.53	612	395	3.81	0.46	7.72
Fe/OMC-0.10	11.45	600	385	3.76	0.43	7.69
Fe/OMC-0.15	12.08	381	256	3.74	0.27	8.34
Fe/OMC-0.20	–	313	201	3.77	0.24	–

[a] Calculated from XRD results using the formula $a = 2(3)^{-1/2}d_{100}$.
[b] Calculated by the BET model from sorption data in a relative pressure range from 0.05 to 0.3.
[c] Estimated from the t-plot method using the Harkins and Jura standard isotherm with the thickness range 3.5–5.0 Å.
[d] Calculated by the BJH model from the desorption branches of the isotherms.
[e] The total pore volume was estimated from the amount adsorbed at a relative pressure of 0.995.
[f] Calculated using the formula $f = a - d$.

carbon nanochannels with a d spacing of about 10 nm can be clearly observed in the images of Fe/OMC-0.05 (Fig. 3a) and Fe/OMC-0.10 (Fig. 3b), which is consistent with small-angle XRD results (9.9 nm). The dark spots with a diameter of 6–20 nm are the iron nanoparticles, which are uniformly embedded in the walls of the OMCs. An orderly arranged strip-like channels structure can be observed in the Fe/OMC-0.10 (Fig. 3c), and only wormhole-like disordered structure can be visualized on Fe/OMC-0.20 (Fig. 3d). As shown in Fig. 4, the HRTEM image of iron nanoparticle embedded in the wall of OMC illustrates the perfect arrangements of the atomic layers and lack of defects. The lattice plane distance in Fig. 4b is 2.03 Å, which is consistent with the [1 1 0] plane of the α-Fe (JCPDS card No. 06-0696) [24,47]. The cell parameters calculated from the TEM images are in good agreement with those (Table 1) calculated from XRD patterns.

Nitrogen sorption isotherms were recorded to investigate the effect of the iron loading content on the pore properties of the Fe/OMC composites. Fig. 5 shows N_2 adsorption–desorption isotherms and the pore size distributions of Fe/OMC-M (M = 0.05, 0.10, 0.15, 0.20). All samples are found to own typical type IV isotherms with an obvious H_1-type hysteresis loop, reflecting the characteristics of mesoporous materials, which are typical adsorption for mesoporous materials with 2D hexagonal ordered structure [25]. The sharp inflections between the relative pressures p/p_0 = 0.4–0.7 in these isotherms correspond to capillary condensation within uniform mesopores. The pore size distribution curves determined by applying BJH method using the desorption branches of the isotherms are shown in Fig. 5b. The curves reveal that the pores of each sample are relatively uniform and centered at around 3.8 nm. Table 1 lists the pore parameters of Fe/OMC composites. As shown in Table 1, Fe/OMC-0.05 has a BET surface area of 612 m^2/g and pore volume of 0.46 cm^3/g. The surface areas and pore volumes of the specimens decreased with the increasing of iron content. However, there is a sharp decrease of surface area and pore volume between Fe/OMC-0.10 and Fe/OMC-0.15 due to the destruction of ordered mesostructure. These N_2 adsorption–desorption data are in well agreement with the small-angle XRD (Fig. 1) and the TEM (Fig. 3) results. The iron content is a critical factor to form well ordered mesoporous structure.

The hysteresis curves of Fe/OMC composites were obtained at room temperature with a vibrating sample magnetometer. The saturation magnetization *Ms*, remanent magnetization *Mr*, and coercivity *Hc* are the main technical parameters to characterize the magnetism of ferromagnetic materials. Fig. 6 shows the magnetic hysteresis loops of Fe/OMC composites with different iron contents. Table 2 lists the magnetic parameters of Fe/OMC composites. As

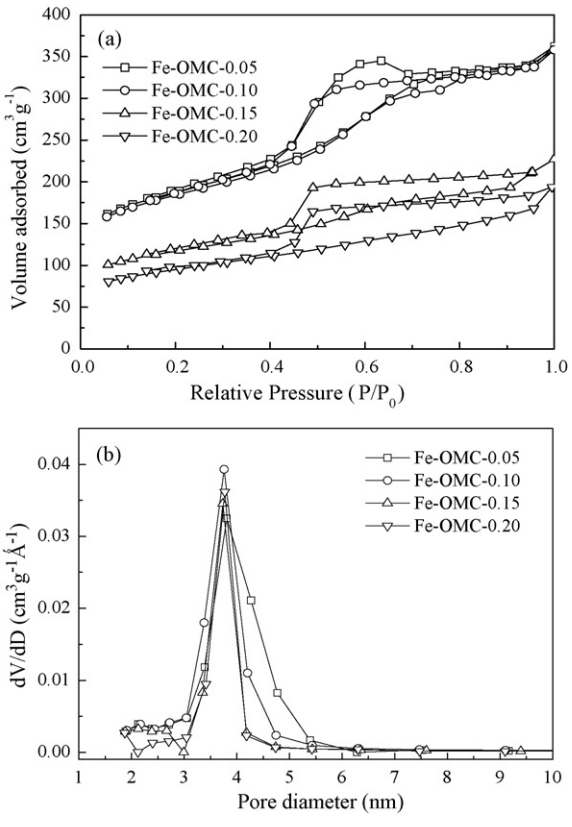

Fig. 5. N_2 adsorption–desorption isotherms (a) and pore size distributions of Fe/OMC composites with different iron loadings (b).

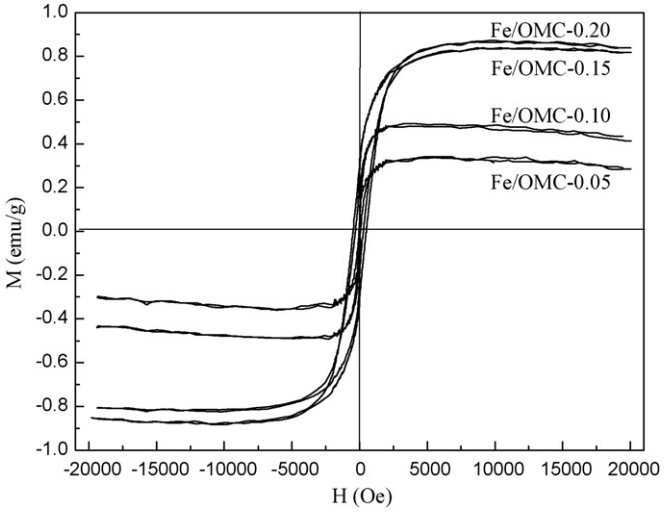

Fig. 6. Magnetization curves of Fe/OMC composites with different iron loadings.

Table 2
Magnetic properties of Fe/OMC composites.

Sample name	*Ms* (emu/g)	*Mr* (emu/g)	*Mr*/*Ms*	*Hc* (Oe)
Fe/OMC-0.05	0.34	0.06	0.18	74
Fe/OMC-0.10	0.48	0.11	0.23	37
Fe/OMC-0.15	0.84	0.29	0.35	305
Fe/OMC-0.20	0.87	0.33	0.38	485

shown in Table 2, with the increases of the iron content, *Ms*, *Mr*, and *Hc* of the Fe/OMC composites increase. The values are much lower than those of bulk iron, which are attributed to the nanosize of the iron particles and the presence of carbon [24]. The lower *Ms*, *Mr* and *Mr*/*Ms* indicate that the Fe/OMC composites exhibited soft ferromagnetic characteristic, which implied many potential applications including ferrofluid technology, magnetocaloric refrigeration and etc. The magnetic separability of the magnetic Fe/OMC composites was tested in an ethanol solution by placing a magnet near the glass bottle. The powder Fe/OMC samples were attracted by the magnet and separated from the solution. The property of magnetic attraction is quite useful for the separation of carbon in catalytic applications [48], electromagnetic wave absorbers [49] and adsorption processes [23].

4. Conclusions

The iron nanoparticles confined in OMCs have been directly synthesized through a simple soft templating method. The iron species were spontaneously reduced to metallic iron nanoparticles during the carbonization process. The carbon material exhibited highly ordered mesoporous structure, and the iron nanoparticles were uniformly confined in the OMC walls. The Fe/OMC composites exhibit the soft ferromagnetic behavior and the magnetization parameters can be adjusted by the content of iron. Moreover, such self-protected Fe/OMC composites will be promising materials for many applications in the fields of separation, catalysis and drug delivery which could be separated by an appropriate magnetic field.

Acknowledgements

This work was supported by the National Natural Science Foundation of China (Grant No. 50672004) and the National High-Tech Research and Development Program (2008AA03Z513).

References

[1] R. Ryoo, S.H. Joo, S. Jun, J. Phys. Chem. B 103 (1999) 7743–7746.
[2] H.J. Shin, R. Ryoo, M. Kruk, M. Jaroniec, Chem. Commun. 4 (2001) 349–350.
[3] M. Kang, S.H. Yi, H.I. Lee, J.E. Yie, J.M. Kim, Chem. Commun. 17 (2002) 1944–1945.
[4] M. Kruk, M. Jaroniec, T.W. Kim, R. Ryoo, Chem. Mater. 15 (2003) 2815–2823.
[5] A.B. Fuertes, Micropor. Mesopor. Mater. 67 (2004) 273–281.
[6] J. Lee, J. Kim, T. Hyeon, Adv. Mater. 18 (2006) 2073–2094.
[7] C.H. Kim, D.K. Lee, T.J. Pinnavaia, Langmuir 20 (2004) 5157–5159.
[8] H. Yang, Y. Yan, Y. Liu, F. Zhang, R. Zhang, Y. Meng, J. Phys. Chem. B 108 (2004) 17320–17328.
[9] H. Song, L. Li, X. Chen, New Carbon Mater. 21 (2006) 374–383.
[10] L. Li, H. Song, X. Chen, Micropor. Mesopor. Mater. 94 (2006) 9–14.
[11] H. Xu, Y. Pan, H. Kou, Y. Zhu, J. Guo, J. Alloys Compd. 502 (2010) L6–L9.
[12] Z. Gu, B. Deng, J. Yang, Micropor. Mesopor. Mater. 102 (2007) 265–273.
[13] J. Lee, S. Jin, Y. Hwang, J. Park, H.M. Park, T. Hyeon, Carbon 43 (2005) 2536–2543.
[14] S.E. Moradi, S. Amirmahmoodi, M.J. Baniamerian, J. Alloys Compd. 498 (2010) 168–171.
[15] J. Ding, K. Chan, J. Ren, F. Xiao, Electrochim. Acta 50 (2005) 3131–3141.
[16] C. Minchev, H. Huwe, T. Tsoncheva, D. Paneva, M. Dimitrov, I. Mitov, M. Fröba, Micropor. Mesopor. Mater. 81 (2005) 333–341.
[17] D. Lee, J. Lee, J. Kim, J. Kim, H.B. Na, B. Kim, Adv. Mater. 17 (2005) 2828–2833.
[18] L. Li, H. Song, X. Chen, Electrochim. Acta 51 (2006) 5715–5720.
[19] W. Xing, S.Z. Qiao, R.G. Din, F. Li, G.Q. Lu, Z.F. Yan, Carbon 44 (2006) 216–224.
[20] T. Wang, X. Liu, D. Zhao, Z. Jiang, Chem. Phys. Lett. 389 (2004) 327–331.
[21] W. Xing, S.Z. Qiao, R.G. Ding, F. Li, G.Q. Lu, Z.F. Yan, H.M. Cheng, Carbon 44 (2006) 216–224.
[22] H. Li, Y. Li, R. Wang, R. Cao, J. Alloys Compd. 481 (2009) 100–105.
[23] J. Yao, L. Li, H. Song, C. Liu, X. Chen, Carbon 47 (2009) 436–444.
[24] J. Li, J. Gu, H. Li, Y. Liang, Y. Hao, X. Sun, L. Wang, Micropor. Mesopor. Mater. 128 (2010) 144–149.
[25] H. Li, H. Xi, S. Zhu, R. Wang, Mater. Lett. 60 (2006) 943–946.
[26] S.H. Joo, S.J. Choi, I. Oh, J. Kwak, Z. Liu, O. Terasaki, Nature 412 (2001) 169–172.
[27] J. Zhou, J. He, Y. Ji, W. Dang, X. Liu, G. Zhao, Electrochim. Acta 52 (2007) 4691–4695.
[28] Z. Ji, S. Liang, Y. Jiang, H. Li, Z. Liu, T. Zhao, Carbon 47 (2009) 2194–2199.
[29] J. Fan, T. Wang, C. Yu, B. Tu, Z. Jiang, D. Zhao, Adv. Mater. 16 (2004) 1432–1436.
[30] I. Grigoriants, L. Sominski, H. Li, I. Ifargan, D. Aurbach, A. Gedanken, Chem. Commun. 7 (2005) 921–923.
[31] X. Dong, W. Shen, J. Gu, L. Xiong, Y. Zhu, H. Li, J. Phys. Chem. B 110 (2006) 6015–6019.
[32] S. Zhu, H. Zhou, M. Hibino, I. Honma, M. Ichihara, Adv. Funct. Mater. 15 (2005) 381–386.
[33] A. Lu, W. Li, A. Kiefer, W. Schmidt, E. Bill, G. Fink, J. Am. Chem. Soc. 126 (2004) 8616–8617.
[34] I.S. Park, M. Choi, T.W. Kim, R. Ryoo, J. Mater. Chem. 16 (2006) 3409–3416.
[35] J. Lee, S. Jin, Y. Hwang, J.G. Park, H.M. Park, T. Hyeon, Carbon 43 (2005) 2536–2543.
[36] X. Dong, H. Chen, W. Zhao, X. Li, J. Shi, Chem. Mater. 19 (2007) 3484–3490.
[37] Y. Cao, J. Cao, M. Zheng, J. Liu, G. Ji, J. Solid State Chem. 180 (2007) 792–798.
[38] A. Lu, H. Tüysüz, F. Schüth, Micropor. Mesopor. Mater. 111 (2008) 117–123.
[39] W. Xing, S. Zhuo, X. Gao, Mater. Lett. 63 (2009) 1177–1179.
[40] J. Yang, F.N. Gu, H.J. Wang, Y. Zhou, J.Y. Yang, Z.Y. Wu, J.H. Zhu, Catal. Today 148 (2009) 88–96.
[41] X. Yuan, W. Xing, S. Zhuo, Z. Han, G. Wang, X. Gao, Z. Yan, Micropor. Mesopor. Mater. 117 (2009) 678–684.
[42] Y. Hou, J.C. Ndamanisha, L. Guo, X. Peng, J. Bai, Electrochim. Acta 54 (2009) 6166–6171.
[43] T. Hiraoka, T. Kawakubo, J. Kimura, R. Taniguchi, A. Okamoto, T. Okazaki, Chem. Phys. Lett. 382 (2003) 679–685.
[44] H. Song, X. Chen, S. Zhang, H. Li, Carbon 41 (2003) 3037–3046.
[45] A. Oberlin, J.P. Rouchy, Carbon 9 (1971) 39–42.
[46] W. Weisweiler, N. Subramanian, B. Terwiesch, Carbon 9 (1971) 755–758.
[47] R.P. Hodgkins, A. Ahniyaz, K. Parekh, L.M. Belova, L. Bergström, Langmuir 23 (2007) 8838–8844.
[48] J. Zhou, J. He, G. Li, T. Wang, D. Sun, X. Ding, J. Zhao, S. Wu, J. Phys. Chem. C 114 (2010) 7611–7617.
[49] L. Xing, J. Qiu, C. Liang, C. Wang, L. Mao, J. Catal. 250 (2007) 369–372.